Construction and Building Materials 304 (2021) 124532

Contents lists available at ScienceDirect

Construction and Building Materials

journal homepage: www.elsevier.com/locate/conbuildmat

# Consolidation of artificial decayed portland cement mortars with an alkoxysilane-based impregnation treatment and its influence on mineralogy and pore structure

I. García-Lodeiro [a,*], R. Zarzuela [b], M.J. Mosquera [b], M.T Blanco-Varela [a]

[a] Eduardo Torroja Institute (CSIC), PO Box 19002, 28080 Madrid, Spain
[b] TEP-243 Nanomaterials Group, Department of Physical-Chemistry, Faculty of Sciences, Universidad de Cádiz, 11510 Puerto Real, Spain

ARTICLE INFO

*Keywords:*
Consolidation
Alkoxysilane
Penetration depth
Porosity
C-S-H gel
Mechanical strength

ABSTRACT

Surface treatments, especially hydrophobic agents to prevent water ingress and consolidants able to fill decay-induced cracks, are often proposed as a method for preserving stone cultural heritage, however its use to protect concrete heritage is much less common. New products, specifically designed for concrete, have been developed. These products are based on alkoxysilanes that interact directly with the products of portland cement (OPC) hydration (essentially $Ca(OH)_2$ and C-S-H) to generate additional C-S-H gel.

This study assesses the effect of an impregnation treatment, based on alkosysilanes, on artificially decayed cement mortars, in terms of product penetration depth, changes in the porosity of mortars and changes in its mechanical strengths. Reduced porosity and enhanced mechanical strength attested to treatment efficacy. Substrate porosity and pore size distribution were not the only factors found to condition treatment effectiveness, however, mineralogical changes caused by the deterioration processes (such as the presence or absence of portlandite, or the presence of salts) modify the sol gelling time and the substrate surface energy, impacting treatment penetration depth.

## 1. Introduction

Concrete structures are known to undergo a number of types of deterioration. Fair-faced concrete is obviously more susceptible to decay than when painted or coated, especially in coastal areas (e.g. rebar corrosion) and regions characterised by extreme day/night temperature differences (e.g. cracking by freeze–thaw cycles, increasing porosity…), severe pollution or the presence of aggressive chemical agents (e.g. black crust formation…)[1-5].

The strategies most commonly deployed today to retard concrete deterioration are implemented during its manufacture and include reducing porosity, lowering the water/cement (w/c) ratio and strengthening the nanostructure with nanoparticles. However, in the case early twentieth century concrete buildings, little heed was paid to the critical parameters that raise the long-term performance of concrete, such as the w/c ratio and the thickness of the concrete cover (in reinforced concrete structures), because decay mechanisms were still poorly understood at the time.

Surface treatments are a used procedure to effectively prevent or retard aggressive substance ingress in concrete [6-10]. The most prominent such treatments include hydrophobic impregnation products that prevent water ingress without blocking pores, protective coatings and impregnation products, that reduce porosity by filling decay-induced pores or cracks and increase the material cohesion (consolidant effect).

For an impregnation treatment to be effective as a consolidant, it must penetrate the damaged substrate's pore system to a sufficient depth to restore the surface properties to their original condition. A proper prediction of the penetration depth on altered materials proves challenging, since it depends not only on the properties of the treatment applied (i.e. viscosity, surface tension, density and polymerization time) but also on the characteristics of the substrate: surface energy, porosity, pore size distribution and composition. Nowadays, the most common products used for consolidation generally have an alkoxysilane, such as tetraethyl-orthosilicate (TEOS) [11-15], whose physical properties favour penetration in most porous materials. Furthermore, research on the surface consolidation of natural stone has fully established that alkoxysilanes perform well in siliceous rock characterised by surface

* Corresponding author.
*E-mail address:* iglodeiro@ietcc.csic.es (I. García-Lodeiro).

https://doi.org/10.1016/j.conbuildmat.2021.124532
Received 23 March 2021; Received in revised form 5 July 2021; Accepted 10 August 2021
Available online 25 August 2021

silanol groups that chemically bond to the treatment, whereas it is less effective in calcareous rock. It is well established [13]that when alcoxysilanes type TEOS, penetrated in a silicon substrate, first undergoes hydrolysis (See Eq. (1)) forming silanol groups (Si-OH) and ethanol , which is easily evaporate without damage in the structure :

$$Si(EtO)_4 + 4H_2O \rightarrow Si(OH)_4 + 4Et(OH)\uparrow \quad (1)$$

After the hydrolysis, condensation takes place inducing the formation and precipitation of an amorphous silica gel that fills the pores in the substrate [13]. In siliceous materials, the hydrolysed silanol groups may interact with the Si-OH groups in the substrate (Supplementary Material), partially restoring the natural binder that fell away during decay and reconnecting loosened mineral grains, with a consolidating effect and an appreciable increase in the material mechanical strength [13].

Characterised by a very particular composition and porosity, concrete differs widely from natural stone. On the one hand, the small diameter of part of its pore system (<100 nm pores) hinders the sol penetration due to the influence of viscous drag forces [16], while on the other hand, the system itself contains a saturated solution of portlandite ($Ca(OH)_2$) and a pH of over 12.5, which greatly accelerates the sol–gel reaction rate (i.e. the sol has less time to advance through the pores). In addition to these factors, the differences between concrete and stone mineralogy can promote different interaction mechanisms with the alkoxysilanes by reaction with the hydration phases, as the exceptionally high pH of the pore solution promotes a high solubility of the hydrolysed $Si(OH)_4$ intermediates (>20 mmol/l at pH 10.5 and quickly increasing in more basic media) [17], which in turn are able to interact with the $Ca^{2+}$ ions [18] and the hydration phases. Recently, we developed an innovative impregnation product consisting on a silica oligomer able to produce new C-S-H gel by polymerization of the silanol groups resulting from the hydrolysis step (Equation (1)) with the $Ca^{2+}$ ions in the pore water in cement, consuming portlandite in the process (Equation (2)), but also able to interact with the C-S-H gel generated in OPC hydration (Equations (3)) [19].

$$Ca(OH)_2 \text{ (OPC hydration)} + Si(OH)_4 \text{ (TEOS hydrolysis)} \rightarrow \text{C-S-H gel} \quad (2)$$

$$\text{C-S-H gel (OPC hydration)} + Si(OH)_4 \text{ (TEOS hydrolysis)} \rightarrow \text{C-S-H gel*} \quad (3)$$

(*more polymerized than the OPC hydration product)

As these C-S-H gels also have free Si-OH groups, their co-condensation with either the $SiO_2$ xerogels or the quartz aggregates by formation of Si-O-Si bonds is expected to increase the cohesiveness of the cementitious materials components. In a similar fashion, the co-condensation reactions can occur between the Si-OH groups and the terminal Al-OH (forming Al-O-Si bonds) from aluminium-containing phases [20], present in the cement matrix (e.g. ettringite, katoite, monocarboaluminate). Additional studies of the alkoxysilanes reactivity in the presence of cement hydration phases [21] revealed that, under high pH conditions, they are able to undergo chemical reaction with Al-containing phases generating new structures, including reticulated aluminosilicate gels in the presence of ettringite, amorphous Al-Si structures with katoite or alumina gels with monocarboaluminate.

Aside from the chemical interactions with the cement matrix, the penetration depth of the impregnation product was thoroughly studied and the correlation between the penetration depth and physical parameters was established using the Monte-Carlo methodology [16].

Although the evaluation of impregnation treatments on healthy cementitious materials is commonplace and can provide a general idea about their effectiveness, it may not be sufficiently representative of their actual field applications, where the concrete structures have suffered structural and chemical changes due to exposure to weathering processes. What is more, concrete structures, depending on the type of decay process, can show different microstructure (porosity and pore size distribution) and mineralogy (presence/absence of secondary phases, such as portlandite). In general, total porosity and mean pore size generally rise with concrete age, favouring the penetration. However, the changes in its mineralogy are not as predictable, since they simultaneously affect factors such as pH, reactivity with the products and surface energy. Predictions on these systems become even more complex when we take into account how decay agents generate a heterogeneous degradation profile through the materials depth, as the extent of alterations/damages depends on factors such as carbonation depth, penetration of the aggressive species, temperature gradients, etc. As such, the mineralogical, physical and chemical properties may not be constant through the whole material. Thus, as these impregnation treatments interact with the products of cement paste hydration, their polymerization rate is affected by pH of the pore solution [11], and their penetration and consolidant effectiveness also depend on the physical/mechanical properties of the substrate, a more thorough understanding is needed of how the consolidant is affected by the ageing-induced changes in C-S-H gel and other compounds resulting from cement hydration, aside from the structural changes.

Starting from this premise, the scope of this paper is to study the performance of an alkoxysilane-based impregnation treatment, synthetized by a surfactant-assisted process described in prior works [22], on artificially decayed mortars, aged by different accelerated processes simulating common decay mechanisms of cementitious materials. These decay mortars will show different microstructure and minerology that would affect its interaction with the impregnation treatment and, therefore, may affect its behaviour and overall performance. This study address the impregnation treatment effectiveness in terms of differences in product uptake and penetration, porosity changes and mechanical performance.

## 2. Experimental

Both the proportion of portland cement in concrete and the composition and particle size distribution of the aggregate used in concrete structures vary widely and depend on material availability at any given worksite in addition to design characteristics. Such concretes share the bonding capacity and strength of the respective cement paste. In this study the system was simplified by preparing and curing a single CEM I-42.5 mortar as recommended in European standard EN-196–1 and exposing the materials to a number of ageing trials. The aim was to modify their mineralogy, microstructure and properties to assess the penetrability and degree of interaction of new alkoxysilane-based treatments in aged specimens.

### 2.1. Preparation of standard OPC mortars

Prismatic OPC mortar specimens ($4 \times 4 \times 16$ $cm^3$) were prepared as specified in European standard EN 196–1 [23] using CEM I 42.5R cement (Table 1), CEN-compliant sand at a ratio of 1/3 and a w/c ratio of 0.5. Although no demoulding product was applied, the inner surface of the mould was coated with a self-adhesive film.

Standard mortars were cured under water at 21 °C for 28 days and then oven-dried at 40 °C for 4 days. These mortars are used as OPC reference (REF).

### 2.2. Ageing

The aforementioned standard mortars were aged using different types of artificial decay processes decay, simulating common decay mechanisms of cementitious materials:

- **Series 1: physical decay-induced ageing**: a) freeze/thaw (F/T) (series 1.1) or (b) wet/dry (W/D) (series 1.2) cycles (in an attempt to crack the mortar)

**Series 2: chemical decay-induced ageing:** a) carbonation (C)

**Table 1**
Chemical composition of Cem I 42.5 (% Oxides in weight) (XRF).

| Oxides | CaO | $Al_2O_3$ | $SiO_2$ | $SO_3$ | MgO | $Fe_2O_3$ | $Na_2O$ | $K_2O$ |
|---|---|---|---|---|---|---|---|---|
| Wt % | 62.98 | 5.63 | 18.72 | 3.05 | 0.87 | 2.68 | 0.04 | 0.85 |
| | **$TiO_2$** | **SrO** | **$Cr_2O_3$** | **Cl** | **ZnO** | **$P_2O_5$** | **LOI[1]** | |
| Wt % | 0.23 | 0.051 | 0.00 | 0.02 | 0.028 | 0.05 | 2.31 | |

Loss of ignition 1000 °C.

(series 2.1); b) sodium chloride crystallization (NaCl) (series 2.2) to simulate decay in monuments located in urban, industrial and coastal areas.

The curing process for these aged mortars was as follows: the mortars for the physical and $Cl^-$ -mediated decay were cured under water at 21 °C for 28 days and then oven-dried at 40 °C for 4 days (same curing process than the OPC reference mortars). Mortars prepared for carbonation-induced ageing were stored in sealed plastic bags at 21 °C for 28 days to ensure 100 % relative humidity and prevent any contact with atmospheric $CO_2$. After the curing mortars were aged using the protocols described briefly below:

- **Series 1.1 freeze/thaw**. Samples were aged in a climatic chamber as specified in standard ASTM C-666 [24]. The 6 h cycles consisted in lowering the temperature from 4 ± 2 °C to –18 ± 2 °C in 0.5 h, keeping the specimens in air at the latter temperature for 2.5 h and then raising the temperature from −18 ± 2 °C to 4 ± 2 °C in 0.5 h, followed by soaking in water at the latter temperature for 2.5 h. Specimens were exposed to a total of 28 cycles, i.e., for 1 week.
- **Series 1.2 wet/dry cycles.** Specimens were soaked in water for 15 h and then oven-dried for 8 h (1 cycle = 15 h in water + 7 h in oven at temperatures higher than 100 °C) [25]. The conditions under which the 145 cycles were performed are listed, in Supplementary Material (SP).
- **Series 2.1 carbonation.** The cured samples were aged in a $CO_2$ incubator at 2 % $CO_2$, 25 °C and Relative Humidity (RH) = 80 % for 4 months, after which they were removed and prepared for characterisation. Although the special curing conditions deployed ensured the mortar specimens exhibited no carbonation front prior to ageing, at the end of the 4 months the front was 10.2 mm deep.
- **Series 2.2 Sodium chloride crystallization**. Mortars were soaked in an NaCl-saturated solution (35.7 g/100 cc $H_2O$) for 48 h and then oven-dried at 105 °C for 24 h [26]. After four full cycles, the specimens were desalinated by soaking in deionised water for 2 weeks, during which the water was refreshed every 24 h.

During ageing the specimens were examined visually and ultrasonic pulse velocity (USV) measurements were taken (supplementary material). In general term, accelerated ageing was detained when a drop in the mechanical strengths was observed (See Untreated mortars in Fig. 1) and/or when the USV reading varied by over 15–20 %. In contrast, given the absence of such change in the wet/dry-aged mortars, in series 1.2 the procedure was continued through a total of 145 cycles.

### 2.3. Characterization of the changes induced by ageing

The mortars aged as described above were subsequently tested for compressive strength on an Ibertest (Autotest-200/10-SW) test frame (3 replicates per series). To characterise the samples a 10 mm thick section was removed from the unbroken half of each specimen along the outer surface exposed to attack (supplementary material). A 1x1x1 $cm^3$ cube was cut out of the 4x1x1 $cm^3$ section and used for microstructural characterisation on a Micrometrics AutoPore IV 9500 V1.09 pore sizer. The samples were soaked for 2 d in isopropanol and subsequently dried in a desiccator (7d) prior to analysis.

In order to obtain an enriched cement paste to facilitate characterization of the hydration phases with less interference from the quartz (sand) aggregate, the remaining part of the section was ground gently [rubbed/tapped] with a rubber cork, after which the larger grains of sand were separated from the resulting powder with an 88 μm sieve, [27]. The enriched fraction so obtained was submerged in isopropanol to detain hydration [28] and stored in sealed containers until characterised.

A portion of the cement powder was attacked chemically to quantify the remaining quartz by diluting 1 g of the said cement powder in 65 ml of 22 v% HCl acid, heated in a sand bath for 10 min. The insoluble residue (IR) filtered out of the sample was then burnt at 1000 °C, weighted and analysed with FTIR to ensure that only quartz remained after the attack (the FTIR spectra for the post-attack residues can be furnished as supplementary material). In this procedure, both the anhydrous cement particles and the hydration products dissolved in the acid or burnt off (the insoluble residue), leaving only quartz from the sand.

The enriched OPC paste remaining was analysed with X-Ray Diffraction (XRD) and Thermogravimetric analysis (TG/DTG) for mineralogy. X-ray diffraction patterns of the powdered samples were recorded on a Philips CuK radiation PW 1730 diffractometer, step-scanning at 2 °C·$min^{-1}$ and a 2θ angle of 2° to 60°, using a 1°

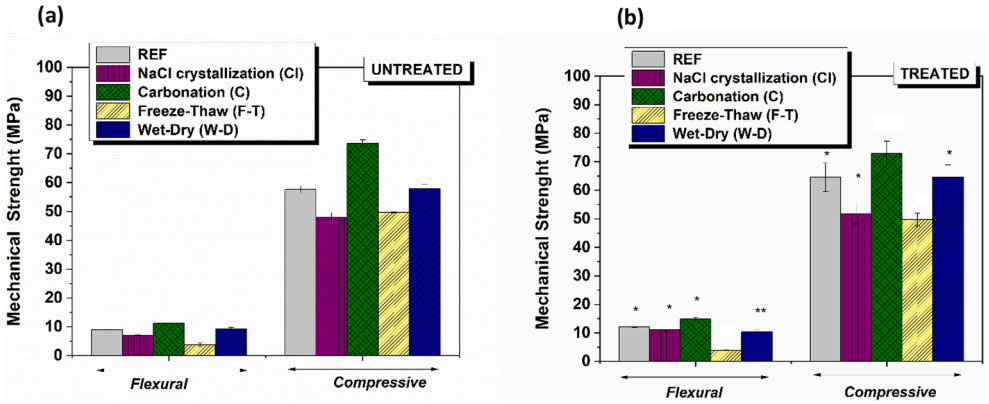


**Fig. 1.** Flexural and compressive strengths in (a) untreated and (b) treated OPC standard and decayed mortars Values where an unpaired *t*-test showed significant differences between treated and untreated mortars are marked with * (p-value < 0.01) and ** (p-value < 0.05).

divergence slit, a 1° anti-scatter slit and a 0.1 mm receiving slit. Thermogravimetric analysis was conducted on a Q600 TA SDT analyser in Pt crucibles (reference, empty crucible) with experimental conditions of 30 °C to 1000 °C in an $N_2$ atmosphere at a flow speed of 5 °C/min.

The changes in the surface energy of the OPC paste were determined through contact angle measurements with two probe liquids of known surface tension: $H_2O$ ($\gamma_l^P = 26.3$ erg·cm$^{-2}$, $\gamma_l^D = 46.5$ erg·cm$^{-2}$) and $CHCl_3$ ($\gamma_l^P = 0.0$ erg·cm$^{-2}$, $\gamma_l^D = 27.5$ erg·cm$^{-2}$). According to the Owens and Wendt theories [29] (i.e. geometric mean approach to the surface free energy), the solid–liquid contact angle can be expressed as a function of their surface energy components through the following equation:

$$(\gamma_s^D \gamma_l^D)^{1/2} + (\gamma_s^P \gamma_l^P)^{1/2} = \gamma_l(\cos\theta + 1)/2$$

$$\gamma_l = \gamma_l^D + \gamma_l^P$$

Where $\gamma_S$ and $\gamma_l$ correspond to the liquid and solid surface energies, and the superscript D and P correspond respectively to their dispersive and polar components. Contact angles were determined by the sessile drop method, using a video-based, software-controlled contact angle analyzer (OCA 15 plus, Data Physics Instruments). In order to minimize the influence of roughness and porosity over the static contact angle (SCA), the samples were prepared by compacting the enriched OPC paste powders into pellets [30].

### 2.4. Synthesis of the impregnation product

The product was synthesised as described in earlier works [19,22]. Briefly, an oligomeric alkoxysilane (Wacker TES40 WN) was mixed at 99.34 v% proportion, with 0.5 v% de-ionized $H_2O$ and 0.16 v% n–octylamine (Sigma-Aldrich), as a catalyst and surfactant, to a total volume of 500 ml. Afterwards, the mixture was blended in a Bandelin Sonopuls HD3200 homogeniser for 10 min at an amplitude of 74 %. According to its specifications, TES40 has an average 5Si-O units chain length and produces $SiO_2$ at a rate of ~ 40 % of the original weight after full polymerization. The resulting sol from the synthesis was stored in an airtight vessel until its application on the substrates.

### 2.5. Treatment of the mortars and evaluation

The impregnation products were applied on both the sound and the artificially aged mortars. Prior to application of the product, all specimen surfaces were polished with P180 sandpaper, rinsed with water to remove any dust and dried at 40 °C to a constant weight. This drying step was considered by taking into account the general recommendations for the field application of alkoxysilane and siloxane-based treatments on buildings, namely: temperature of 0–30 °C, air humidity of 20–90% and minimizing water content of the substrate, as it can hinder product absorption [31]. The product was sprayed in different layers onto the surface at a pressure of 2 bar at 2 s intervals until no further product was absorbed after 10 min, deemed as an indication of saturation. Uptake was determined as the difference in weight before and after application per area unit.

The influence of the mortars mineralogy over polymerization rate of the product was studied by mixing the enriched OPC paste powders (see section 2.3) with the freshly synthetized product (0.07 g powder per 1 ml product) and, after homogenization of the dispersions by mechanical stirring, casting 0.5 ml volumes in Ø 2 cm plates. Gel time was determined visually as the point where the sol stops behaving as a fluid.

After application, the treated mortars were left to cure at room conditions (20 °C, 40% RH) for 28 days, which corresponds to the recommended time to ensure polymerization reactions of the product are complete.

Penetration depth of the product on the different mortars was studied through qualitative analysis of Scanning electron microscopy (SEM) micrographs (registered in secondary electrons mode) of cross-sectional cuts, using a NanoSEM 450 microscope from the FEI Company, working at an acceleration voltage of 2.5 kV. Prior to the analysis, the samples were gold sputtered with a 5 nm thick layer. For this purpose, the penetration depth was estimated based on the morphological changes, observing where the structure became more compact and typical morphologies of the polymerized sol [32] or its reaction products with the cementitious matrix [19] were identified. Elemental analysis of the Ca/Si ratio by energy-dispersive X-ray spectroscopy (EDX) or micro X-ray fluorescence (μ-XRF) was deemed inconclusive due to interference of the aggregate and the similarity between the alkoxysilane reaction products and the cementitious matrix phases.

Porosity changes after the treatment application were evaluated through Mercury Intrusion Porosimetry (MIP). For this purpose, a 4–5 mm thick section was removed from the specimens along the treated surface. This sampling section was determined based on the lowest penetration values observed by SEM (i.e. in carbonated specimens), in order to ensure only regions where the product is present were analyzed. Fragments of this section were cut and used for microstructural characterisation.

Finally, the consolidant performance of the treatment was evaluated by measuring the mechanical strengths (flexural and compressive) of the 16x4x4 cm$^3$ specimens, according to UNE-EN 196–1 standard [23].

## 3. Results and discussion

### 3.1. Characterization of the artificially decay mortars.

As it has been point out, the penetration and the uptake of the impregnation treatment will be dependent on the characteristics of the substrate (surface energy, porosity, pore size distribution and composition). Therefore, a proper characterization of the mortars before to apply the impregnation treatment (untreated mortars), not only from a microstructural point of view, but also from a mineralogical side, is essential to understand the future performance of the treatments. Changes in the properties of the mortars after the decay processes are shown below:

#### 3.1.1. Mechanical strenghts

Fig. 1(a) shows the flexural and compressive strengths of the aged mortars to the values for the untreated reference mortar. The freeze/thaw (F/T) and sodium chloride (NaCl crystallization) aged samples exhibited lower mechanical strength than the reference. In contrast, mechanical strength was higher in the specimens exposed to carbonation than in the reference, as expected because the $CaCO_3$ resulting from the reaction between $Ca(OH)_2$ and $CO_2$ filled the pores, producing a more compact cementitious material [33-35]. Contrary to expectations, wet/dry treatment not only induced no significant strength loss in the mortars, but after 145 cycles the flexural and compressive mechanical strengths shown similar values than the OPC reference which were 9 ± 0.32 MPa and 57.45 ± 1.14 MPa respectively (Fig. 1(a)).

#### 3.1.2. Porosity and pore size distribution

Table 2 gives the porosity data for the reference and decayed mortars (Untreated samples). The post-ageing pore size distribution for all four series and the reference are depicted in Fig. 2.

Total porosity increased in the F/T and W/D samples relative to the reference mortar (REF) (from ~ 12 % in REF to 14.55 % in F/T and 14.76 % in W/D). The series 1.1 samples exhibited obvious frost damage, attested to by pore size redistribution (Fig. 2). Ice induced damage by enlarging the pores, favouring water ingress in the microstructure which raised its saturation coefficient and with it the risk of further freeze/thaw damage [36]). Whilst the 0.1 to 0.01 μm range prevailed in the reference mortar, the F/T mortars exhibited two dominant ranges: 1 μm to 0.1 μm and 0.1 μm to 0.01 μm (Fig. 2).

The greatest rise in the proportion of pore size fractions in W-D mortars was observed for pores ranging from 10 μm to 1 μm and 1 μm to

**Table 2**
Total porosity in aged and reference mortars (untreated and treated).

| | | Mercury intrusion porosimetry values (MIP) | | | | | |
|---|---|---|---|---|---|---|---|
| | | REF | Series 1.1 Freeze- thaw (F-T) | Series 1.2 Wet-dry (W-D) | Series 2.1 Carbonation (C) | | Series 2.2 NaCl Crystallization (NaCl) |
| Untreated | Total porosity (%) | 11.98 | 14.55 | 14.76 | 9.11 ($C_{out.}$) | 11.34 ($C_{in.}$) | 11.89 |
| Treated | Total porosity (%) | 9.81 | 12.39 | 10.40 | 6.39 | – | 10.37 |
| Total porosity reduction | | 18.12↓ | 14.86 ↓ | 29.53 ↓ | 24.25 ↓ | – | 12.82 ↓ |

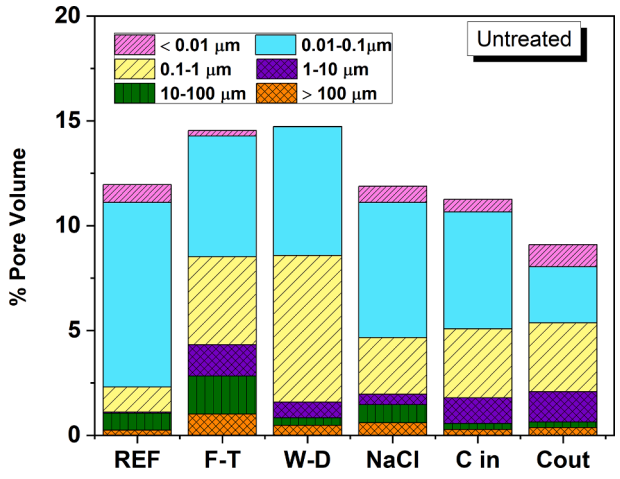


**Fig. 2.** Total porosity and pore size distribution (vol. % of pores) in reference and decayed OPC mortars (untreated samples) (outermost 10 mm) (**Legend:** REF: reference; F-T: freeze–thaw; W-D: wet-dry; Cl: NaCl. NaCl crystallization; Cin: carbonation (iner); Cout: carbonation (outer)).

0.1 μm (Fig. 2). That rise may have been associated with temperature-mediated ettringite decomposition, as discussed below in connection with the mineralogical characterisation of the mortar (Fig. 3), and the resulting five-fold reduction in the volume occupied by its crystals. The decline in the proportion of the pores < 0.01 μm in these mortars, associated with C-S-H, denoted alterations in gel structure. Changes in temperature may have also induced microcracking and portlandite may have partially dissolved during the test as a result of specimen moistening, further contributing to a rise in porosity.

Despite the rise in porosity and the change in pore size distribution, mechanical strength remained essentially unchanged (Fig. 1(a)). The explanation for that apparent discrepancy may lie in the existence of two competing processes. On the one hand, porosity rose with mortar dissolution, expansion and contraction, and ettringite decomposition whilst on the other the experimental conditions (fairly high temperature and 15 h soaking per cycle) favoured hydration of the remaining anhydrous portland cement particles. That in turn generated more C-S-H gel, offsetting the effect of greater porosity.

The behaviour in chemically aged mortars was completely different. No significant change was observed in total porosity (Table 2) in mortars exposed to $Cl^-$ penetration (series 2.2). A number of studies [37,38] has shown that the two mechanisms involved in the damage induced in concrete soaked in NaCl solutions are $Ca^{2+}$ leaching and salt crystallisation. Low NaCl concentrations may favour leaching, whereas at high concentrations it may be hindered due to lower portlandite solubility [39]. Given that here the mortars were soaked in a saturated NaCl solution, leaching was unlikely. Changes in porosity might have been mediated by the formation of Friedel's salt, which would fill the voids, altering the pore size distribution (Fig.s 2). Salt crystallisation may have a dual effect, filling pores and thereby enhancing mechanical strength, while inducing microcracking (Friedel's salt) that would weaken the OPC paste [37]. In this study no substantial changes were observed in porosity in the $Cl^-$-aged mortar, while mechanical strength declined slightly, possibly as a result of salt formation.

As noted in the methodology, the mortars prepared for carbonation were cured differently from the other specimens. In series 2.2, two areas of the specimens were analysed, the outer portion ((between the surface and the carbonation front, clearly defined by applying phenolphthalein, 10.2 mm from the external surface) and the non-carbonated inner

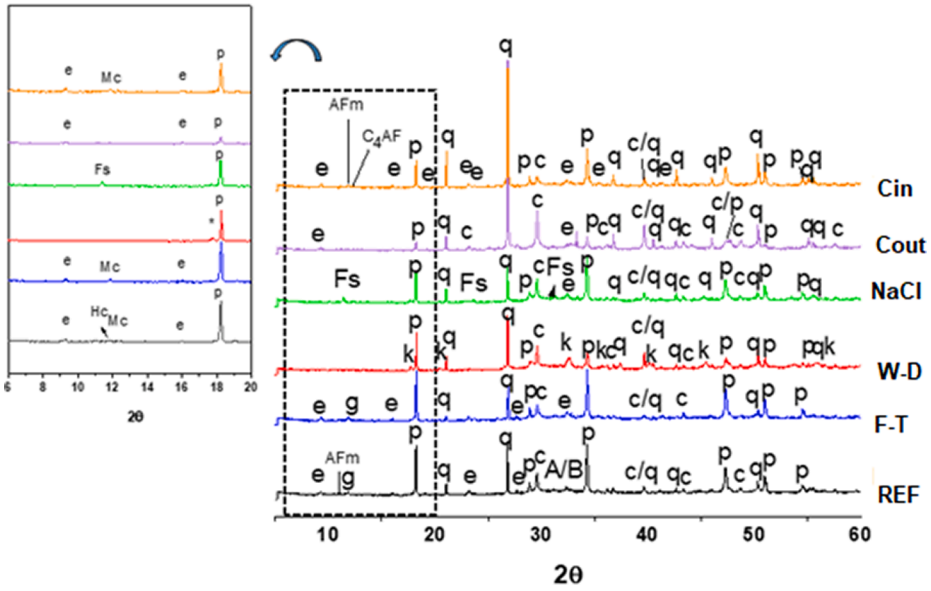


**Fig. 3.** XRD patterns for OPC pastes in the reference (REF) and aged mortars (**Legend:** e: ettringite ($Ca_6Al_2(SO_4)_3(OH)_{12}{\cdot}26H_2O$) (COD 9012922); Hc: hemicarboaluminate ($Ca_8Al_4CO_{16}{\cdot}22H_2O$) (COD 2007668); Mc: monocarboaluminate ($Ca_4Al_2(CO_3)(OH)_{12}{\cdot}5H_2O$ (COD 2007668) p: portlandite ($Ca(OH)_2$) (COD 9000113); q: quartz ($SiO_2$) (COD 9005017); B: belite ($C_2S$) (COD 1540704); c: calcite ($CaCO_3$) (COD 9000113); Fs (Friedeĺs salt ($Ca_2Al(OH)_6(Cl,OH){\cdot}2H_2O$) (COD 9009353) (k:Silicon substituted katoite/hydrogarnet; $Ca_3Al_2(SiO_4)(OH)_8$ (COD 1–084-0917).

portion. As expected, porosity was lower in the carbonated than in the non-carbonated area (Table 3). Pore size distribution changes with respect to the one observed in the outer portion; The 0.1 μm to 0.01 μm range, predominant in the inner mortar, was considerably reduced in the outer area (Fig. 2), while the volume of pores lower than 0.01 μm increases . This increase in the proportion of smaller pores can be explained due to larger pores are filled by the precipitation $CaCO_3$, as a result of the reaction between $Ca(OH)_2$ and $CO_2$ [35] as well as by the increase of CSH content.

### 3.1.3. Mineralogy

The mineralogical and microstructural changes induced by ageing (prior to impregnation treatment application) were analysed with XRD and TG/DTG. The findings are discussed below. The XRD patterns for the decayed and reference mortars are reproduced in Fig. 3. The diffractogram for the reference OPC contained signals indicative of secondary hydration products such as portlandite ($Ca(OH)_2$), ettringite (e) ($Ca_6Al_2(SO_4)_3(OH)_{12}{\cdot}26H_2O$), and the AFm phases hemicarboaluminate (Hc) ($Ca_8Al_4CO_{16}{\cdot}22H_2O$) and monocarboaluminate ($Ca_4Al_2(CO_3)(OH)_{12}{\cdot}5H_2O$), as well as of anhydrous particles (primarily belite) present in the original cement. Diffraction lines for calcite were also identified and attributed to both the mineral present in the anhydrous cement and the reaction between portlandite and atmospheric $CO_2$.

Despite the efforts made to separate the sand from the OPC paste, reflections attributable to quartz were observed in all samples. Even with traces of quartz in the enriched samples, rest of anhydrous clinker and several types of hydration products are perfectly identifiable.

The pattern for the F/T-aged mortars was nearly identical to the trace for the reference, the sole difference being the absence of Hc. In contrast, the diffractogram for the W/D mortars varied substantially from the reference: no ettringite or AFm was detected, (which justify the increase in the total porosity observed by MIP) whilst a new poorly crystallised phase, katoite-hydrogarnet, with empirical formula $Ca_3Al_2(SiO_4)(OH)_8$, appeared. Crystallising in the cubic system, that phase is isostructural with katoite ($Ca_3Al_2(OH)_{12}$), although with the replacement of four OH groups with one $SiO_4$ group the unit cell size is smaller (12.5727 Å vs 12.358 Å). The diffraction lines for this phase were shifted relative to those for pure katoite and their intensities differed. By way of example, the first reflection associated with this katoite-hydrogarnet (211) at around $2\theta = 17.56°$ had a d value of 5.04 (at intensity 37), compared to 5.13 in katoite (at intensity 90). In addition, the wide base of the reflections on the diffractogram for the former denoted poor crystallisation.

No ettringite was detected in the $Cl^-$ aged sample and the only AFm phase observed was in the form of Friedel's salt. Although ettringite is stable in a much wider range of sulfate concentrations than the salt, at high chloride concentrations the field of stability of the latter broadens, whilst that of ettringite and portlandite narrows. Ettringite destabilises at chloride concentrations over 5.658 mol/kg [40].

The outer (up to the carbonation front) area of the C-aged sample was much more highly carbonated than the inner. The substantially lower intensity of the portlandite diffraction lines confirmed that carbonation proceeded normally. Ettringite was identified in both areas, however in the external part the intensity of the reflections are lower than in the inner part, possibly indicating its partial deterioration due to the action of the $CO_2$ [41]. Monocarboaluminate was detected in the inner area only (Fig. 3).

The TG and DTG curves for the reference and the experimentally aged pastes are reproduced in Fig. 4(a) and Fig. 4(b) respectively. Percentage weight loss by temperature interval is given in Supplementary Material, along with portlandite and calcite content in per cent (Fig. 5). The data in the table are the estimated and consequently semi-quantitative result of recalculations performed to factor in the percentage of quartz found in the samples pursuant to the chemical attack described in the methodology (Supplementary Material).

The TG curves (Fig. 4(a)) for most of the aged samples followed the same pattern as in the reference, the exception being the curve for the outer area of the sample exposed to carbonation. Total weight loss differed from one sample to another, however, with the highest value observed in the outer area of the carbonated mortar and the lowest in the W/D mortar (Table SP4).

Some of the peaks on the DTG curves were similar in all the mortars (Fig. 4(b)). The signals located between 66 and 100 °C were associated with ettringite decomposition and the loss of free water and chemically/physically bound water in hydrated products (mostly C-S-H gel) [41]. The intense peak at around 150 °C was attributed to the loss of water in the AFm phases detected with XRD (hemi- and monocarboaluminates) [41], whilst the signal at 446 °C was indicative of $Ca(OH)_2$ dehydroxylation ($Ca(OH)_2 \rightarrow CaO + 2H_2O$) [42,43]. The group of signals at 600 to 750 °C was associated with $CaCO_3$ decarbonation ($CaCO_3 \rightarrow CaO + CO_2$) [42,43]. The slight weight loss in the interval 750 °C to 1000 °C observed in all samples might be indicative of decarbonation of a highly crystallised calcite present in the anhydrous OPC (most of the curves had a low intensity peak at around 867 °C, possibly generated by calcite [41,42]).

The highest percentage of portlandite was found for the F/T sample (Fig. 5). Although given the nature of the W/D procedure the respective specimens were expected to contain a similar amount of the mineral, the actual content was much lower than in the reference mortar. In light of the similarity of the percentage of $CaCO_3$ in the W/D and reference samples, no carbonation seems to occur during W/D ageing. The substantial difference in portlandite content suggests that some of the compound may have solubilised during soaking.

Furthermore, the peaks normally appearing between 60 and 150 °C associated with free water and physically/chemically bound water in hydrated OPC products (essentially C-S-H + AFm + Aft) were virtually absent in this group, an indication that wet/dry ageing had a heavy impact on these phases also. Three signals were detected in the W/D samples: one at 386 °C, (dehydroxylation of scantly crystallized katoite detected by XRD), a second at 446 °C (portlandite dihydroxylation) and a third at 714 °C (calcite decarbonation [41,42]).

The signals at 116 and 317 °C on the DTG curve for the $Cl^-$ penetration-aged sample but not on the reference curve were attributed to the decomposition of Friedel's salt [44]. The percentage of portlandite was slightly lower in this sample than in the reference (17.33 vs 19.35 %). Friedel's salt may form via dissolution/precipitation as a result of the reaction between sodium chloride, calcium hydroxide and aluminates ($C_3A$) as in Equation (4):

$$2NaCl + Ca(OH)_2 + 3CaO.Al_2O_3 + 10H_2O \rightarrow 3CaO.CaCl_2.Al_2O_3{\cdot}10H_2O + 2Na^+ + 2OH– \quad (4)$$

and/or of interaction with sulfoaluminate phases (ionic exchange between chlorides in the pore solution and the sulfate ions in hydrated monosulfoaluminate $C_3A{\cdot}CaSO_4{\cdot}12H_2O$) [45]. As part of the portlandite was consumed and no AFm phases were detected, salt formation was attributed to a combination of the two processes. In the former, the $OH^-$ ions released during its formation would hinder calcium leaching, particularly at high NaCl concentrations such as used here (NaCl

**Table 3**
Uptake ($g/m^2$) and Penetration depth (mm) of thee consolidant in the OPC mortars.

| Type of mortar | Uptake ($g/m^2$) | Estimated Penetration depth (mm) (1) |
|---|---|---|
| **OPC Reference (REF)** | 501.2 ± 85.5 | ≤8 mm |
| **Freeze-Thaw (F-T)** | 2289.9 ± 52.2 | ≤15 mm |
| **Wet-Dry (W-D)** | 467.3 ± 53.5 | ≤8 mm |
| **NaCl Crystallization (NaCl)** | 818.8 ± 113 | ≤12 mm |
| **Carbonation (C)** | 652.0 ± 58.6 | ≤5 mm |

Based on SEM analysis.

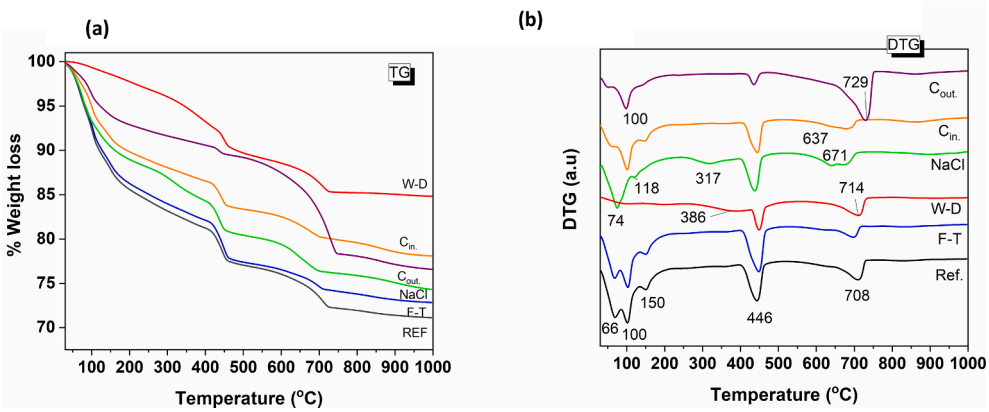


**Fig. 4.** (a) TG and (b) DTG curves for aged samples (W-D: wet-dry; NaCl: NaCl crystallization ; F-T: freeze–thaw; $C_{out.}$: carbonation (outer area); $C_{in.}$: carbonation (inner area); REF: reference).

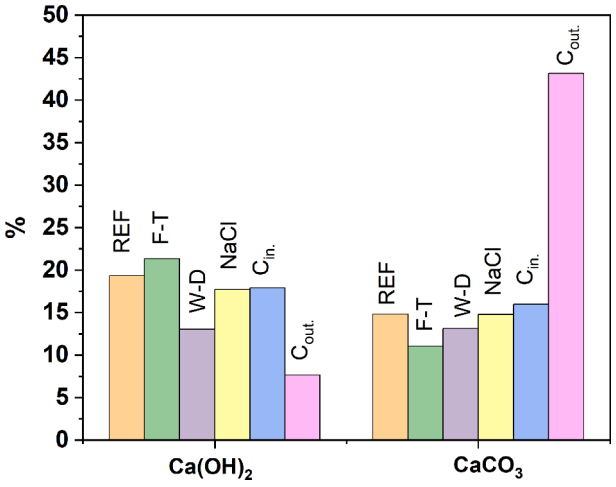


**Fig. 5.** Estimated percentage (%) of portlandite and $CaCO_3$ formed in decayed mortars.

saturated solution) . In a recent paper Wang et al. [38] proved that the mechanical deterioration of specimens in NaCl solutions (0.5 wt (wt) % to 20 wt% of NaCl) was due to calcium leaching. In this study, however, where ageing was conducted in a supersaturated NaCl solution where portlandite loss resulting from calcium leaching was not significant, strength loss might be explained by internal microcracking induced by salt crystallisation.

The carbonated samples exhibited the behaviour expected under the experimental conditions. The endo peak at 444 °C on the DTG curve associated with portlandite dehydroxylation was much less intense in the carbonated (outer) than the non-carbonated (inner) area of the sample (7.66% vs 17.90%, Fig. 5). The peak at 675 °C in the inner area associated with carbonate decalcification shifted to 729 °C in the outer area. That, together with the substantially greater intensity of the peak (from 15.98% to 43.15%) and the minor loss of water at temperature lower than 200 °C confirmed severe carbonation not only of $Ca(OH)_2$ but perhaps also of C-S-H gel and ettringite.

In summary, depending on the type of deterioration process, the mortar microstucture (porosity and pore distribution) and mineralogy are very different. This would condition the interaction concrete substrate-impregnation treatment.

### 3.2. Sol uptake in the mortar and feasibility of interaction with OPC hydration products

Data on impregnation product uptake ($g/m^2$) and estimated penetration depth (mm) in both the reference and decayed OPC mortars are given in Table 3. As noted earlier, product penetration depth in the mortars was estimated via SEM analysis of sample cross-sections. The respective micrographs are reproduced in Supplementary Material.

The SEM micrographs of the treated mortar cross-sections at lower magnification show in general a more compact/cohesive structure compared to their untreated counterparts, which gradually becomes less compact at deeper levels, down to a point where differences cannot be observed (corresponding to the values reported in Table 3). A similar behaviour, where the alkoxysilane-based product penetrates following a gradient, has also been observed by quantitative techniques (FTIR and XRF) on a homogeneous limestone substrate [46]. In addition to this possible concentration gradient, the influence of the aged mortars heterogeneity cannot be completely ruled out since qualitative analysis by SEM may not be sensitive enough to detect their chemical or porosity variations at different depths (i.e. the untreated mortars showed a similar aspect through the first 10 mm). It is worth mentioning that this same aspect limits the sensitivity of the method at detecting the product in larger depths.

The SEM micrographs at higher magnification evidence the coexistence of various reaction products in the consolidated structure at different depths, as well as differences between the product interaction with aged mortars. In all mortars but the chloride-aged ones, the region closer to the surface presents dense particulate structures (part. Size < 100 nm), which are consistent with the structure of the $SiO_2$ xerogels formed by auto-condensation of the product [19]. In the case of the reference mortar and chloride aged ones, needle-like and foil-like structures are observed, which could indicate the formation of C-S-H gel by reaction of the product with portlandite. At larger depths, other morphologies consistent with C-S-H gel can be distinguished (i.e. fibre-like, "Sheaf of wheat", flake-like), as well as structures without a defined morphology, which may be associated to the amorphous reaction products of the product with other cementitious phases [21]. Anyways, the exact nature of the reaction products in the aged mortars cannot be accurately determined without additional techniques. The formation of different phases through the mortar depth can be associated to several factors: (1) differences in the exposure to moisture and water content in the pores. (2) The exact phase composition may vary with depth in the aged mortars. (3) As mentioned before, the product penetrates following a concentration gradient, which implies different the Ca/Si ratios in the pore solution, affecting the structure of the hydration products.

A priori, high total porosity and large pore size diameter would be expected to favour product penetration and therefore the likelihood of

its interaction with the mortar to form a more compact structure of $SiO_2$ and C-S-H gels. The lack of any straightforward relationship between total porosity and product penetration (supplementary material), however, appears to suggest that pore size distribution and the differences in mineralogical composition are more relevant factors. In mortars exposed to freeze/thaw ageing, the uptake was four- to five-fold higher than in the reference while penetration depth was estimated the double (Table 3), which is higher than expected if only the increase in total porosity is accounted for (c.a. 20%). This behaviour can be explained by the changes in pore size distribution, which resulted in a decrease of the smaller sizes (<100 nm) and the apparition of a large proportion in the 1–10 μm range (See Fig. 2), which play a more prominent role in the sol absorption, as studied in previous works combining theoretical and experimental approaches [16]. In order to explain this trend it should be considered that, although the Laplace pressure, the driving force behind capillary suction, is inversely proportional to the pore radius, the opposing viscous drag forces (due to interactions with the pore wall) become more relevant for smaller pores, promoting a pressure drop inversely proportional to $r^2$ (equations are presented in supplementary material).

On the other hand, the wet/dry aged mortars, whose total porosity was practically as high as the freeze/thaw aged ones, presented no significant differences in uptake nor in penetration depth respect to the reference. One of the factors contributing to this behaviour is the different pore structure created by the ageing processes. Unlike the freeze–thaw ageing, the pores created after wet-dry cycles fell predominantly in the 0.1–1 μm range (See Fig. 2), where the contribution to the sol absorption is comparative low. Furthermore, although there is an increase in the 1–10 μm pores, their effect may be partially compensated by the drop observed in the slightly larger pores (10–50 μm). This influence of the pore size is in fact illustrated by the almost linear trend observed for the uptake respect to the % porosity in the micrometric range (Supplementary Material). Penetration depth values, on the other hand, present a more irregular behaviour that may be attributed to factors such as pore shape and the existence of preferential paths.

Nevertheless, these changes alone would not sufficiently explain the low penetration/uptake values, especially considering that the total % porosity in the micron range is fairly similar to the reference mortar. A likely explanation lies on the mineralogical changes experienced by the mortar, which may modify the reactivity and interaction of the product with the substrate. More specifically, these changes may modify two critical parameters: (1) the surface energy of the mortar, which determines the contact angle with the sol (i.e. cos θ in Eq. (5)), (2) the rate of the polymerization reactions, which determines at which point the sol stops being able to flow through the pores [47,48]. As presented in Table 4, the surface energy of the mortar increased with the ageing process, likely due to the lower amount of ettringite and portlandite, which present a lower surface energy than C-S-H gel [21]. This should decrease the contact angle and favour penetration. However, the observed gel time of UCA-T in the presence of the wet/dry aged mortars was faster than with the reference (Table 5). According to prior works [16], where we determined through a sensitivity analysis using Monte-Carlo method, that the relative influence of these two factors depends on the pore size, gel time plays a more prominent role on pores < 10 μm (the majority of the contributions in the wet-dry aged mortars).

**Table 4**
Surface energy of the reference and selected decayed mortars, measured by the sessile drop method on the cementitious matrix powders.

| Type of mortar | $\gamma^d$ (erg/cm$^2$) | $\gamma^p$ (erg/cm$^2$) | $\gamma$ (erg/cm$^2$) |
|---|---|---|---|
| **OPC Reference (REF)** | 26.6 | 20.9 | 47.5 |
| **Wet-Dry (W-D)** | 26.9 | 28.7 | 55.6 |
| **NaCl Crystallization (NaCl)** | 27.0 | 31.9 | 58.9 |
| **Carbonation (C)** | 27.2 | 42.2 | 69.4 |

* $\gamma^d$: dispersive component; $\gamma^d$: polar component.

**Table 5**
Gel time of the UCA-T sol in presence of the cementitious matrix powders (0.07 g powder per ml).

| Type of mortar | Gel time (h) | [b]$\triangle$t (%) |
|---|---|---|
| **OPC Reference (REF)** | 14.0 | 0.0 |
| **Wet-Dry (W-D)** | 13.2 | −5.7 |
| **NaCl Crystallization (NaCl)** | 12.7 | −10.5 |
| **Carbonation (C)** | 14.8 | 5.6 |
| [a]**UCA-T** | 16.0 | 12.5 |

[a] Control, in absence of the mortar powders [b]Respect to gelification in presence of the OPC reference.

The chemically aged mortars, and in particular chloride aged samples, were penetrated more deeply than the controls (in line with the higher uptake values, See Table 4). In a similar fashion to the physically altered mortars, the minor increase in total porosity does not suffice to explain the penetration depths observed. Additionally, although the ageing process induced the formation of some pores in the 1–10 μm, the high penetration suggests that changes in composition and/or hydrated phase microstructure have indeed a higher influence. As seen in Table 4, the formation of polar phases such as Friedel's salt promotes an increase in the surface energy, which is expected to favor penetration (i.e. decreases contact angle). Meanwhile, gel time is faster than the reference or even the wet-dry aged mortars. Nevertheless, in contrast with the wet-dry aged mortars, the contribution of > 10 μm pores is higher for the $Cl^-$ altered mortars. Coincidentally, our prior Monte-Carlo analysis [16] showed that, starting from this pore size, the influence of gel time quickly drops while the contact angle plays a more important role.

The lower penetration observed in the carbonated mortars, on the other hand, could be mainly associated to their lower porosity, caused by partial blockage of the pores with precipitated calcite. These changes are especially evident near the surface, where the influence over capillary absorption of the treatment is higher. In contrast with the mortars aged by wet-dry cycles, the influence of porosity seems to offset the contribution of mineralogical/composition changes for the carbonated mortars (i.e. their higher surface tension and lower pH should theoretically increase penetration depth).

Substrate microstructure is not the only parameter involved in the interaction with the treatment, however. Decay-induced changes in the mineralogy of the latter also play a role, as it has been discussed in this section. Mineralogical characterisation of the mortars revealed such changes, which included declines in portlandite content (XRD and TG/DTG findings); the formation of new phases such as Friedel's salt after Cl attack and katoite after wet/dry cycles; and the alteration of C-S-H gel chemical composition and nanostructure after carbonation. The presence or absence of these secondary cement hydration phases would condition not only the type of chemical interaction with the treatment and gelling kinetics, but also modify substrate surface energy, with the concomitant impact on product penetration.

As the principle underlying these new treatments is their interaction with hydration products such as portlandite to form more C-S-H gel, the smaller the amount of portlandite (as in carbonated systems), the smaller the possible interaction with the treatment. The interaction mechanism would therefore be expected to differ: i.e., in the absence of portlandite the impregnation product might polymerise, releasing silica gel only and therefore behaving as in traditional substrates such as stone. Nonetheless, same authors have recently proved that such treatments also interact with C-S-H gel in ways that would very likely differ depending on gel Ca/Si ratio and mean chain length (MCL)[21]. Other phases present, such as Friedel's salt and katoite, might also interact with the impregnation treatment [21]. All these factors would condition both the degree of penetration and the penetration depth of the treatment.

### 3.3. Evaluation of the porosity and mechanical strengths after the application of the impregnation treatment

Assessment of post-treatment mortar porosity (Fig. 6) revealed a 12 % to 30 % reduction, depending on mortar type and degree of decay, confirming the efficacy of the treatment in the outermost 5 mm. In contrast with the product uptake and penetration values, the steepest declines in total porosity were observed in the mortars aged by wet-dry cycles and carbonation. That apparent discrepancy might be attributable to the method used to analyse the samples. In all cases, MIP analysis was conducted in the outermost 4 mm to 5 mm of the mortar. In the W-D and carbonated samples, with lowest penetration and uptake, the product would concentrate predominantly near the surface. That effect was consistent with the SEM findings (Supplementary Material), where the

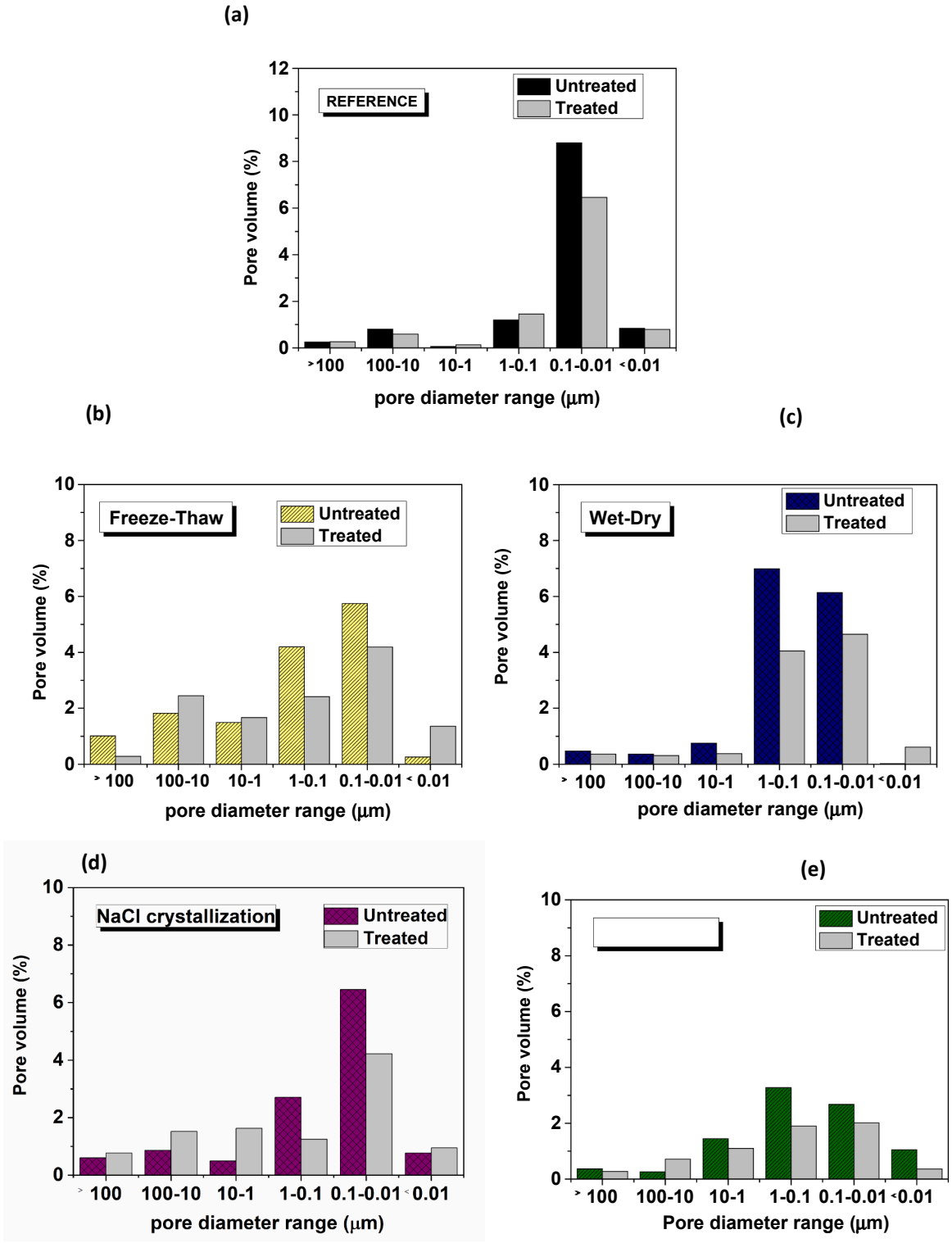


**Fig. 6.** Pore volume (%) in each pore size fraction before and after applying the treatment to the **(a)** reference **(b)** freeze–thaw **(c)** wet-dry **(d)** NaCl and **(e)** carbonated mortars.

structure in that zone of the W-D and C mortars was observed to be more compact than in the analogous zone in the freeze–thaw- and chloride-aged materials.

Material porosity has been reported to be altered by the treatment due to the deposition of an active agent in the open pores, raising microporosity provided the macropores (>10 μm) are partially filled [49]. That in turn would favour a decline in resistance to freeze–thaw-prompted decay and salt crystallisation, for the smaller the pore size, the higher is crystallisation pressure [50]. The situation differed in the mortars treated here. On the whole, the pore volume of each range remained practically constant in the reference mortar, except for a decline in pore volume observed in the 0.1 μm to 0.01 μm range, corresponding to the capillary pores in the cementitious matrix (Fig. 6), and the one which represents the majority of the pore volume of this material (>80%).

On the other hand, for all the aged mortars, a substantial reduction after treatment was observed for the sub-micrometric pores in the 1 μm to 0.1 μm range, aside from a decrease in the 0.1 μm to 0.01 μm ranges (Fig. 6) similar to the reference mortar. Contrary to expectations, a slight rise, which was particularly significant in the freeze–thaw- and chloride-aged mortars, was observed in the proportion of the largest pores in some cases, especially in the 10 μm to 100 μm range.

In particular, pores in the 1 μm to 0.1 μm fraction appeared to be the ones predominantly filled by the alkoxysilane-based impregnation treatment on all aged mortars. This observation is consistent with the behaviour of alkoxysilane-based products on porous rocks, where a number of authors found that their effect was greater in pores ~ 1 μm than in those smaller or larger [51,52]. Similar behaviour was observed by Barberena et al. [53,54] in cement mortars consolidated with TEOS products. Those authors reported TEOS-based treatments to reduce capillary porosity in mortar, in particular the smallest such pores (1 μm to 0.01 μm), most effectively. These observations can be partially explained by the behavior of the pores regarding capillary absorption [16]. The larger pores generally have a low contribution towards the product absorption, since capillary forces (i.e. Laplacian pressure) are inversely proportional to pore radius. On the other end, the absorption in extremely small pores is hindered by the interactions with the pore wall (i.e. viscous drag forces). In addition to the aforementioned factors, the small size makes this pores more susceptible to be blocked/filled by the reaction products.

That reduction in the proportion of the smallest pores would favour pore structure refinement (as a result of physical filling [55]) and consequently enhance durability by obstructing the diffusion of aggressive ions.

Another noteworthy observation is that most of the mortars exhibited a minor rise in pore volume in the < 0.01 μm range (C-S-H gel pores: Fig. 6), possibly resulting from the C-S-H formed as a reactio products between the alkoxysilane and portlandite [53]. In contrast, this effect was not observed for the carbonated mortars, as the proportion of portlandite in them and the pH are significantly lower. Barberena et al. [53,54] recorded similar results for mortars consolidated with TEOS, nanosilica and lime.

The final pore size distributions of the treated mortars (Fig. 7) may be attributed to how the product penetrates through the materials and the structure observed in the cross-section cuts by SEM (Supplementary Material). On the one hand, the contribution of the smallest pores (<0.01 μm) follows a similar trend as the uptake, which is consistent with presence of the reaction products with pores in that range (i.e. C-S-H gel, $SiO_2$ xerogel…). On the other hand, the porosity of the chloride and freeze–thaw aged mortars in the 0.01–1 μm range is lower than for the wet-dry aged ones. Taking into account that this pore ranged is where a highest decrease was observed, these observations are in line with the trend observed for product uptake.

For the reference mortar, however, the pore volume distribution is shifted towards the 0.01–0.1 μm region, which is expected considering the scarce presence of larger pores in the untreated mortar.

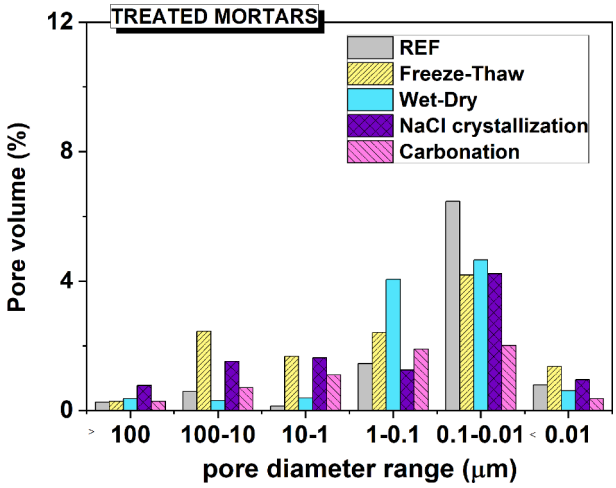


**Fig. 7.** Pore volume (%) in each pore size fraction after applying the treatment to the Reference, Freeze-Thaw, wet-dry, NaCl crystallization and carbonated mortars.

The larger pores (>1 μm), however, follow the opposite trend compared to the smaller ones, showing a higher proportion on the mortars where the product presented higher uptake (freeze–thaw and chloride). This can be explained considering that their larger size makes them less susceptible to blockage by the reaction products, in line with the structure observed in the SEM micrographs (Supplementary material) where larger voids are visible for the treated freeze–thaw and chloride aged mortars.

The lower porosity and higher cohesion manifested as a general increase in the mechanical strength (flexural and compressive) of the mortars (Fig. 1(a) and (b) respectively), although the trend cannot be described solely in terms of product penetration nor total porosity reduction. Flexural and compressive strength variations showed a similar behavior, although the former was noticeably more affected by the application of the treatment, likely because it is more affected by the contact between zones of different properties (i.e. the interior is less altered than the interior) and their tendency towards crack propagation [56]. With the exception of the freeze–thaw aged mortars (where no significant increase was observed), penetration depth/uptake of the product promoted a higher increase of the mechanical strength, with moderate increases for the carbonated and wet-dry specimens and a significant increase in the flexural strength of the reference and chloride aged ones (recovering the strength of the original material in the latter). In these cases, a higher proportion of the product is expected to increase the cohesion of the material, as the reaction products are able to form chemical bonds with the cementing phases [19] and/or the siliceous aggregate [7], and the presence of larger pores is relatively small. In contrast, the freeze–thaw aged mortars did not experience significant strength changes after the treatment despite the high penetration and uptake values. As previously discussed, freeze–thaw ageing causes physical damages manifested as the formation of larger pores (>10 μm) and 0.1–0.3 mm cracks and (Supplementary Material), which severely affect the mechanical strengths. After the treatment, the product filled the smaller pores more effectively while it has a lower efficiency at filling the > 10 μm pores and said cracks, which are the main cause of the low mechanical performance of the mortar. The low (non-significant) increase in compressive strength of the carbonated mortar, on the other hand, can be attributed to the lower product penetration and the already high resistance of the untreated material.

## 4. Conclusions

The consolidant effect of the impregnation treatment has been evaluated through its ability to fill the pores of the mortars and its

modification of their mechanical properties, two of the factors which prevent, respectively, the ingress of decay agents in the structure and the damages associated with their action mechanisms. As expected, changes in the microstructure but also in the mineralogy of mortars, consequence of the decay process, condition the degree of uptake and the penetration depth of the treatment in the substrate.

- The alkoxysilane-based treatment effectively consolidates OPC mortars, reducing total porosity and raising mechanical strength due to the formation of a $SiO_2$ gel and hydration products (e.g. C-S-H gel) inside the pore structure. However, the results from the freeze–thaw aged mortars show that consolidating effectiveness is severely decreased for materials with wider cracks (0.1–0.3 mm).
- Impregnation product uptake and depth of penetration is higher in the mortars where the ageing processes generates pores in the 0.1–1 μm range (i.e. freeze–thaw and chloride ingress), rather than the ones with a higher total porosity. This behavior is associated to the balance between capillary and viscous drag forces. Conversely, the pore volume reduction predominantly occurs by filling of the pores in the 1 μm to 0.1 μm range by the alkoxysilane-based product.
- Pore structure alone does not fully explain product uptake and penetration for all altered mortars, as the mineralogical changes caused by some ageing processes modify key parameters involved in capillary absorption. More specifically, the presence or absence of secondary cement hydration products such as portlandite or AFm phases and apparition of new phases (e.g. calcite from carbonation or Friedel's salt from chloride ingress) modifies the surface tension of the solid, which determines the contact angle of the liquid with the pore wall. On the other hand, the changes in pH associated to these mineralogical changes affect the kinetics of the product polymerization.

## Declaration of Competing Interest

The authors declare that they have no known competing financial interests or personal relationships that could have appeared to influence the work reported in this paper.

## Acknowledgements

This work has received funding from the European Union's Horizon 2020 - Research and Innovation Framework Programme under grant agreement No 760858 (Innovaconcrete project). Funding from the Regional Government of Madrid (TopHeritage-CM; S2018/NMT_4372) is also gratefully acknowledged. Finally, the support by the Spanish Government/FEDER-EU (MAT 2017-84228-R) is also acknowledged.

## Appendix A. Supplementary material

Supplementary data to this article can be found online at https://doi.org/10.1016/j.conbuildmat.2021.124532.

## References

[1] K. Kovler, V. Chernov, Failure, Distress and Repair of Concrete Structures 2 - Types of damage in concrete structures Woodhead Publishing Series in Civil and Structural Engineering 2009, 32-56.
[2] G. De Schutter, Damages to Concrete Structures, CRC Press, Taylor & Francis Group, Boca Raton, USA, ISBN: 978-0-415-60388.
[3] Z. Bonić, G.T. Ćurčić, N. Davidović, J. Savić, Damage of Concrete and Reinforcement of Reinforced-Concrete Foundations Caused by Environmental Effects, Procedia Eng. 117 (2015) 411–418.
[4] F.P Glasser, J., Marchand, E. Samson, Durability of concrete Degradation phenomena involving detrimental chemical reactions, Cement and Concrete Research, 38 [2](2008) 226-246.
[5] X. Pan, Z. Shi, C. Shi, T.-C. Ling, N. Li, Tung Chai Ling, Ning Li, A review on concrete surface treatment Part I: Types and mechanisms, Constr. Build. Mater. 132 (2017) 578–590.
[6] Publication Date (15/12/2004.).
[7] L. Shen, H. Jiang, T. Wang, K. Chen, H. Zhang, Performance of silane-based surface treatments for protecting degraded historic concrete, Prog. Org. Coat. 129 (2019) 209–216.
[8] M. Sánchez, P. Faria, L. Ferrara, E. Horszczaruk, H.M. Jonkers, A. Kwiecień, J. Mosa, A. Peled, A.S. Pereira, D. Snoeck, M. Stefanidou, T. Stryszewska, B. Zając, External treatments for the preventive repair of existing constructions: A review, Constr. Build. Mater. 193 (2018) 435–452.
[9] X. Pan, Z. Shi, C. Shi, T.-C. Ling, N. Li, A review on concrete surface treatment Part I: Types and mechanisms, Constr. Build. Mater. 132 (2017) 578–590.
[10] Haibing Zheng, Weihua Li, Fubin Ma, Qinglin Kong,The effect of a surface-applied corrosion inhibitor on the durability of concrete, Construction and Building Materials 37(2012) 24(3), 299-307.
[11] G. Wheeler G. Alkoxysilanes and the consolidation of stone. The Getty Conservation Institute, 2005.
[12] A.M. Barberena-Fernández, P.M. Carmona-Quiroga, M.T. Blanco-Varela, Interaction of TEOS with cementitious materials: Chemical and physical effects, Cem. Concr. Compos. 55 (2015) 145–152.
[13] Franco Sandrolini, Elisa Franzoni, Barbara Pigino, Ethyl silicate for surface treatment of concrete – Part I: Pozzolanic effect of ethyl silicate, Cem. Concr. Compos. 34 (3) (2012) 306–312.
[14] Barbara Pigino, Andreas Leemann, Elisa Franzoni, Pietro Lura, Ethyl silicate for surface treatment of concrete – Part II: Characteristics and performance, Cem. Concr. Compos. 34 (3) (2012) 313–321.
[15] P. Maravelaki-Kalaitzaki, N. Kallithrakas-Kontos, D. Korakaki, Z. Agioutantis, S. Maurigiannakis, Evaluation of silicon-based strengthening agents on porous limestones, Prog. Org. Coat. 57 (2006) 140–148.
[16] Janez Perko, Rafael Zarzuela, Inés Garcia-Lodeiro, María Teresa Blanco-Varela, Maria J. Mosquera, Timo Seemann, Li Yu, Li Yu, The importance of physical parameters for the penetration depth of impregnation products into cementitious materials: Modelling and experimental study, Constr. Build. Mater. 257 (2020) 119595, https://doi.org/10.1016/j.conbuildmat.2020.119595.
[17] S. Wilhelm, M. Kind, Influence of pH, temperature and sample size on natural and enforced syneresis of precipitated silica, Polymers (Basel). 7 (2015) 2504–2521, https://doi.org/10.3390/polym7121528.
[18] A.A. Hamouda, H.A.A. Amiri, Factors affecting alkaline sodium silicate gelation for in-depth reservoir profile modification, Energies. 7 (2014) 568–590, https://doi.org/10.3390/en7020568.
[19] Rafael Zarzuela, Manuel Luna, Luis M. Carrascosa, María P. Yeste, Inés Garcia-Lodeiro, M. Teresa Blanco-Varela, Miguel A. Cauqui, José M. Rodríguez-Izquierdo, María J. Mosquera, Producing C-S-H gel by reaction between silica oligomers and portlandite: A promising approach to repair cementitious materials, Cem. Concr. Res. 130 (2020) 106008, https://doi.org/10.1016/j.cemconres.2020.106008.
[20] G. Wheeler, Alkoxysilanes and the Consolidation of Stone, The Getty Conservation Institute, Los Angeles, California (2005), https://doi.org/10.1007/s13398-014-0173-7.2.
[21] I. Garcia-Lodeiro, P. Carmona-Quiroga, R. Zarzuela, M.J. Mosquera, M.T. Blanco-Varela, Chemical Interaction between synthetic pure OPC hydrated phases and an alkoxysilane-based impregnation treatment, Cem. Concr. Res. (2021) 142 106351, https://doi.org/10.1016/j.cemconres.2020.106351.
[22] Dario S. Facio, Manuel Luna, Maria J. Mosquera, Facile preparation of mesoporous silica monoliths by an inverse micelle mechanism, Microporous Mesoporous Mater. 247 (2017) 166–176.
[23] UNE EN 196-1-2000. Methods of testing cement - Part 1: Determination of strength.
[24] ASTM C666. Standard Test Method for Resistance of Concrete to Rapid Freezing and Thawing.
[25] Juan M. Manso, Juan A. Polanco, Milagros Losañez, Javier J. González, Durability of concrete made with EAF slag as aggregate, Cem. Concr. Compos. 28 (6) (2006) 528–534.
[26] S. Martínez Ramírez, Desarrollo de nuevos morteros de reparación resistentes al ataque biológico. Empleo de la sepiolita como material soporte de los biocidas, Ph. D Thesis (1995). Universidad Complutense de Madrid (UCM).
[27] D. Gaspar-Tebar, J.L Sagrera-Moreno, V. Gonzalez-Vila, M. Marin-Bohorouez, Durabilidad del hormigón: Acción del agua de mar sobre un cemento portland resistente a los sulfates. Influencia de la adición de escorias y de cenizas volantes, Materiales de Construccion, 224 (1991) [41] 57-71.
[28] F. Winnefeld, A. Schöler, B. Lothenbach, Sample preparation (Chapter 1) in A Practical Guide to Microstructural Analysis of Cementitious Materials, Ed. Karen Scrivener, Ruben Snellings, and Barbara Lothenbach CRC Press (2016) Taylor & Francis Group.
[29] D.K. Owens, R.C. Wendt, Estimation of the surface free energy of polymers, J. Appl. Polym. Sci. 13 (1969) 1741–1747.
[30] A. Alghunaim, S. Kirdponpattara, B.M.Z. Newby, Techniques for determining contact angle and wettability of powders, Powder Technol. 287 (2016) 201–215, https://doi.org/10.1016/j.powtec.2015.10.002.
[31] M. Bofeldt, B. Nyman, Penetration depth of hydrophobic impregnating agents for concrete / Eindringtiefe von Hydrophobierungsmitteln in Beton, Restor. Build. Monum. 8 (2014) 217–232, https://doi.org/10.1515/rbm-2002-5663.
[32] Juan F. Illescas, Maria J. Mosquera, Producing surfactant-synthesized nanomaterials in situ on a building substrate, without volatile organic compounds, ACS Appl. Mater. Interfaces. 4 (8) (2012) 4259–4269.
[33] J.F. Young, R.L. Berger, J. Breese, Accelerated curing of compacted calcium silicate mortars on exposure to $CO_2$, J. Am. Ceram. Soc. 57 (1974) 394.
[34] M FERNANDEZBERTOS, S SIMONS, C HILLS, P CAREY, A review of accelerated carbonation technology in the treatment of cement-based materials and sequestration of $CO_2$, Journal of Hazardous Materials B 112 (3) (2004) 193–205.

[35] A. Wieczorek, M. Koniorczyk, The influence of type of cement on the degradation of microstructure and transport properties of cement.
[36] W. Li Wenting, M. Pour-Ghaz, J. Castro, J. Weiss, Water Absorption and Critical Degree of Saturation Relating to Freeze-Thaw Damage in Concrete Pavement Joints, Journal of Material, Civ. Eng. 24 (3) (2012) 299–307.
[37] Yi Wang, Tamon Ueda, Fuyuan Gong, Dawei Zhang, Meso-scale mechanical deterioration of mortar due to sodium chloride attack, Cem. Concr. Compos. 96 (2019) 163–173.
[38] K. Wang, D.E. Nelsen, W.A. Nixon, Damaging effects of deicing chemicals on concrete materials, Cem. Concr. Compos. 28 (2) (2006) 173–188.
[39] S. Chandra, A. Xu, Influence of presaturation and Freeze-Thaw test conditions on length changes of portland cement mortar, Cem. Concr. Res. 22 (4) (1992) 515–524.
[40] D. Damidot and F.P. Glasser: Thermodynamic investigation of the CaO-Al2O3-CaSO4-CaCl2-H2O system at 25°C and the influence of Na2O. Proceedings of the 10th International Congress on the Chemistry of Cement (ICCC 1997) (Gothenburg, Sweden) 4 (1997), 4iv066.
[41] Haemin Song, Yeonung Jeong, Sungchul Bae, Yubin Jun, Seyoon Yoon, Jae Eun Oh, Jae Eun Oh, A study of thermal decomposition of phases in cementitious systems using HT-XRD and TG, Constr. Build. Mater. 169 (2018) 648–661.
[42] B. Lotenchabac, P. Durdzinski, K. De Weerdt, Thermogravometric analysis in A Paractical Guide to Micrstructural Analysis of Cementitious Materials, Ed by K, R. Snellings and B. Lothenbach, CCR press, Taylor and Francis Book, Scrivener, 2016.
[43] M. Földvári, Handbook of thermogravimetric system of minerals and its use in geological practice, Published by the Geological Institute of Hungary, Budapest, 2011.
[44] R. Lannegrand, G. Ramosy, R. Talero, Condition of knowledge about the Friedel salt, Materiales de Construcción 51 (2001) 63–71.
[45] V. Baroghel-Bouny, X. Wang, M. Thiery, M. Saillio, F. Barberon, Barberon Paris, Prediction of chloride binding isotherms of cementitious materials by analytical model or numerical inverse analysis, Cem. Concr. Res. 42 (9) (2012) 1207–1224.
[46] M.L. Almoraima Gil, Manuel Luna, Rafael Zarzuela, M. Valme García-Moreno, Quantitative determination of the penetration of a silica-based consolidant in a limestone by FTIR spectroscopy, Vib. Spectrosc. 110 (2020) 103109, https://doi.org/10.1016/j.vibspec.2020.103109.
[47] H.R. Pakravan, M. Jamshidi, M. Latifi, Relationship between the surface free energy of hardened cement paste and chemical phase composition, J. Ind. Eng. Chem. 20 (4) (2014) 1737–1740.
[48] Christian Perruchot, Mohamed M. Chehimi, Marie-Josèphe Vaulay, Karim Benzarti, Characterisation of the surface thermodynamic properties of cement components by inverse gas chromatography at infinite dilution, Cem. Concr. Res. 36 (2) (2006) 305–319.
[49] J.L. Perez, R. Villegas, J.F. Vale, M.A. Belllo, M. Alcalde, Effects of consolidant and water repellent treatments on the porosity and pore size distribution of limestones" en ICCROM, International Colloquium Methods of Evaluating Products for the Conservation of Porous Building Materials in Monuments, 203–211, Roma, 1995.
[50] R. Fort, Tratamientos de conservación y restauración de geomateriales: tratamientos de consolidación e hidrofugación", La conservación de los geomateriales utilizados en el patrimonio, Programa Geomateriales, (2012) Madrid: 125-132.
[51] F. Elhaddad, L.A.M. Carrascosa, M.J. Mosquera, Long-Term Effectiveness, under a Mountain Environment, of a Novel Conservation Nanomaterial Applied on Limestone from a Roman Archaeological Site, Materials 11 (2018).
[52] P. Maravelaki-Kalaitzaki, N. Kallithrakas-Kontos, D. Korakaki, Z. Agioutantis, S. Maurigiannakis, Evaluation of silicon-based strengthening agents on porous limestones, Prog. Org. Coat. 57 (2) (2006) 140–148.
[53] A.M. Barberena-Fernández, M.T. Blanco-Varela, P.M. Carmona-Quiroga, Use of nanosilica- or nano lime-additioned TEOS to consolidate cementitious materials in heritage structures: Physical and mechanical properties of mortars, Cem. Concr. Compos. 95 (2019) 271–276.
[54] A.M. Barberena-Fernández, Conservacion de esculturas de Hormigon: efecto de consolidantes en pastas y morteros de cemento, Thesis work, 2015, Universidad Complutense de Madrid (UCM) , Madrid, Spain.
[55] P. Houa, X. Chenga, J. Qian, S.P. Shahd, Effects and mechanisms of surface treatment of hardened cement-based materials with colloidal nano $SiO_2$ and its precursor, Constr. Build. Mater. 53 (2014) 66–73.
[56] L. Toniolo, A. Paradisi, S. Goidanich, G. Pennati, Mechanical behaviour of lime based mortars after surface consolidation, Constr. Build. Mater. 25 (4) (2011) 1553–1559.